Journal of Ceramic Processing Research. Vol. 14, No. 3, pp. 292~296 (2013)

J O U R N A L O F
Ceramic Processing Research

Properties and consolidation of nanostructured TiO_2 by pulsed current activated sintering

In-Jin Shon[a,*], Geon-Woo Lee[a], Jung-Mann Doh[b] and Jin-Kook Yoon[b]

[a]*Division of Advanced Materials Engineering and the Research Center of Advanced Materials Development, Engineering College, Chonbuk National University, 561-756, Republic of Korea*

[b]*Interface Control Research Center, Korea Institute of Science and Technology, PO Box 131, Cheongryang, Seoul 130-650, Republic of Korea*

TiO_2 powders were high-energy ball milled for various durations and consolidated using the pulsed current activated sintering (PCAS). The effect of milling on the sintering behavior and crystallite size TiO_2 powders were evaluated. A nanostructured dense TiO_2 compact with a relative density of up to 99% was readily obtained within 1 min. The ball milling effectively refined the crystallite structure of TiO_2 powders and facilitated the subsequent consolidation. The sinter-onset temperature was reduced appreciably by the prior milling for 10 h. Accordingly, the relative density of TiO_2 compact increased as the milling time increases. The microhardness and fracture toughness of sintered TiO_2 increased as the density increases.

Key words: Nanomaterials, Sintering, Mechanical Properties, TiO_2.

Introduction

TiO_2 is a widely employed material due to important technological applications in photocatalytic and photoelectric devices, chemical sensors and optical coatings.[1-4] TiO_2 presents three crystalline structures: brookite, anatase and rutile. The most common are anatase and rutile, since brookite is rather unstable. Submitting TiO_2 to high thermal treatments provokes the transformation of anatase to rutile, which is the thermodynamically stable phase at high temperatures. The different phases can affect several properties of titania, such as the catalytic activity or the gas sensing response [5].

Nanostructured materials have been widely investigated because they demonstrate wide functionality and exhibit enhanced or different properties compared to bulk materials [6, 7]. Particularly, in the case of nanostructured ceramics, the presence of a large fraction of grain boundaries can lead to unusual or better mechanical, electrical, optical, sensing, magnetic, and biomedical properties [8-14]. In recent days, nanocrystalline powders have been developed by the thermochemical and thermomechanical process named the spray conversion process (SCP), co-precipitation and high energy milling [15-17]. However, the grain size in sintered materials becomes much larger than that in pre-sintered powders due to the rapid grain growth during a conventional sintering process. So, controlling grain growth during sintering is one of the keys to the commercial success of nanostructured materials. Unconventional sintering techniques, including high-pressure densification, magnetic pulse compaction and shock densification, have been proposed to overcome the problem of grain growth [18-20]. However, these methods have failed to provide fast, reproducible techniques that yield large quantities of high density samples with nanostructured grains.

The pulsed current activated sintering (PCAS) method has recently emerged as an effective technique for sintering and consolidating high temperature materials [21, 22]. PCAS is similar to traditional hot-pressing, but the sample is heated by a pulsed electric current that flows through the sample and a die. This process increases the heating rate (up to 2000 °K minute^{-1}) to a degree much higher than that of traditional hot-press sintering.

In this study, we investigated the sintering of TiO_2 by the PCAS method. The goal of this research is to produce nanopowder and dense nanostructured TiO_2 material. In addition, we also studied the effect of high energy ball milling on the sintering behavior, crystallite size and mechanical properties of TiO_2.

Experimental Procedure

The anatase titanium oxide powder used in this research was supplied by Alfa, Inc. The powder had a grain size of -325 mesh and was reported to be 99.6% pure. The powder was first milled in a high-energy ball mill (Pulverisette-5 planetary mill) at 250 rpm for various time periods (0, 1, 4, and 10 h). Tungsten carbide balls (9 mm in diameter) were used in a sealed cylindrical stainless steel vial under an argon atmosphere. The

*Corresponding author:
Tel : +82-63-270-2381
Fax: +82-63-270-2386
E-mail: ijshon@chonbuk.ac.kr

weight ratio of balls-to-powder was 30 : 1. Milling resulted in a significant reduction in the particle size. The crystallite size of TiO_2 powders was calculated from the full width at half-maximum (FWHM) of the diffraction peak by Suryanarayana and Grant Norton's formula [23] :

$$B_r\ (B_{crystalline} + B_{strain})\ \cos\theta = k\ \lambda / L + \eta \sin\theta \qquad (1)$$

where B_r is the full width at half-maximum (FWHM) of the diffraction peak after instrumental correction; $B_{crystalline}$ and B_{strain} are FWHM caused by small grain size and internal stress, respectively; k is a constant (with a value of 0.9); λ is wavelength of the X-ray radiation; L and η are the grain size and internal strain, respectively; and θ is the Bragg angle. The parameters B and B_r follow Cauchy's form with the relationship: $B = B_r + B_s$, where B and B_s are the FWHM of the broadened Bragg peaks and the standard sample's Bragg peaks, respectively.

The TiO_2 powders were placed in a graphite die (outside diameter, 35 mm; inside diameter, 10 mm; height, 40 mm) and then introduced into the pulsed current activated sintering system (Eltek Co., Korea). A schematic diagram of this method is shown in Fig. 1. The system was first evacuated and a uniaxial pressure of 80 MPa was applied. An pulsed current (on time; 20 μs, off time; 10 μs) was then activated and maintained until the densification rate was negligible, as indicating by the observed shrinkage of the sample. Sample shrinkage is measured in real time by a linear gauge measuring the vertical displacement. Temperatures were measured by a pyrometer focused on the surface of the graphite die. At the end of the process, the pulsed current was turned off and the sample was allowed to cool to room temperature. The process was carried out under a vacuum of 40 mtorr (5.33 Pa).

The relative density of the sintered sample was measured by the Archimedes method. Microstructural information was obtained from product samples, which had been polished and etched using thermal etching for 1 h at 950 °C. Compositional and microstructural analyses of the products were made through X-ray diffraction (XRD), field emission scanning electron microscope (FE-SEM) with energy dispersive spectroscopy (EDS). Vickers hardness was measured by performing indentations at a load of 10 kg and a dwell time of 15s.

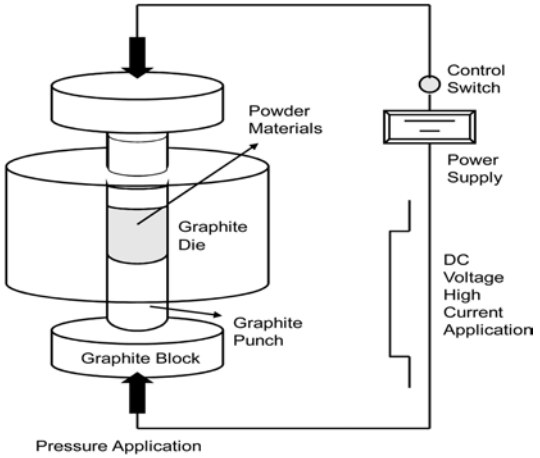

Fig. 1. Schematic diagram of the apparatus for the pulsed current activated sintering (PCAS).

Results and Discussion

Effect of milling on crystallite size

The high-energy milling refined the microstructure of TiO_2 particles. Fig. 2(a-d) shows X-ray diffraction patterns of the TiO_2 powders after milling for 1 - 10 hrs. The broadening of TiO_2 peaks due to crystallite refinement and strain is evident after milling for 1 h, and it continuously broadened during the prolonged milling. The milling process is known to introduce impurities from the ball and/or container. However, in this study, peaks other than TiO_2 were not identified. SEM images of Fig. 3(a-d) show the particle size reduction occurred during the high-energy milling process. The TiO_2 crystallite size by Suryanarayana and Grant Norton's formula was reduced to 70, 31, and 20 nm by milling for 1, 4, 10 h, respectively. The crystallite size reduction was most pronounced during the 1st hour of milling.

Effect of milling on sintering-start temperature

Fig. 4 shows the shrinkage record of TiO_2 compacts under the applied pressure of 80 MPa. In all cases, there was a brief thermal expansion period as soon as the pulsed current was applied. After the initial expansion, the shrinkage displacement increases with heating time and the start of the continuous shrinkage

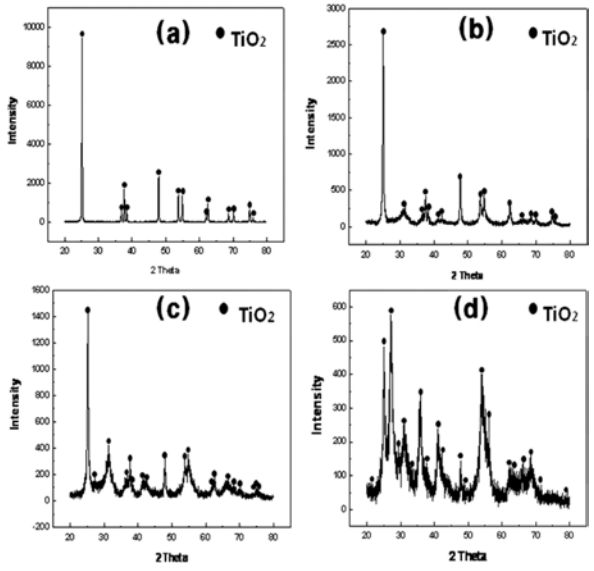

Fig. 2. X-ray diffraction patterns of the TiO_2 powders after high-energy milling for various durations : (a) as-received (b) milled for 1 h, (c) milled for 4 h, and (d) milled for 10 h.

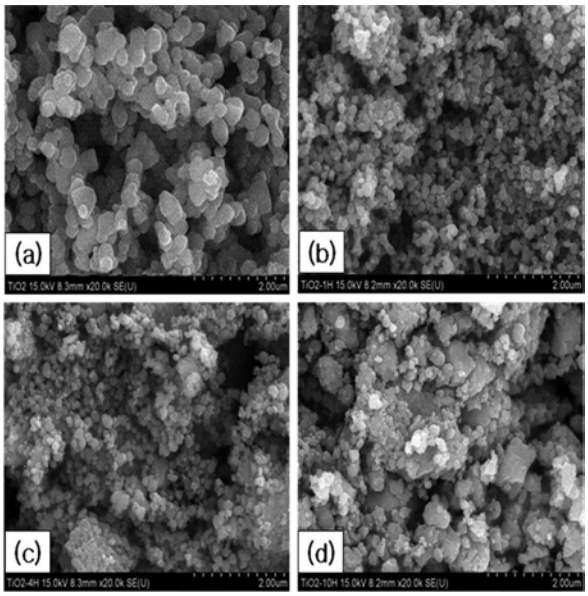

Fig. 3. SEM micrographs of TiO_2 powders after milling for various durations: (a) as received, (b) 1 h, (c) 4 h, and (d) 10 h.

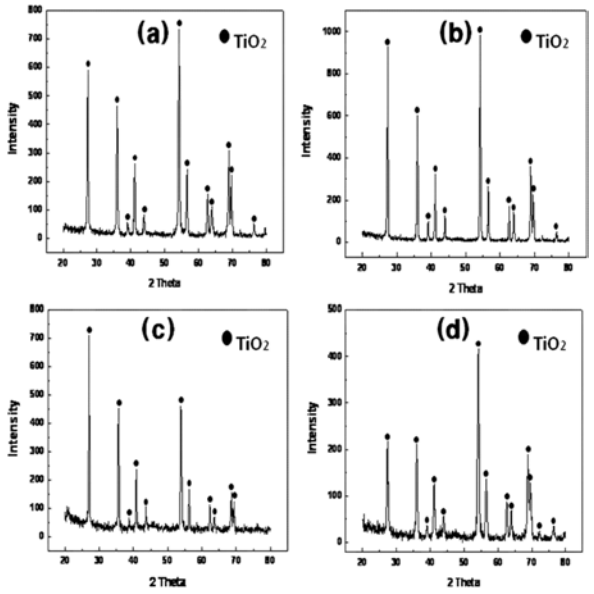

Fig. 5. X-ray diffraction patterns of the sintered compact using TiO_2 powders after milling for various durations : (a) as-received (b) milled for 1 h, (c) milled for 4 h, and (d) milled for 10 h.

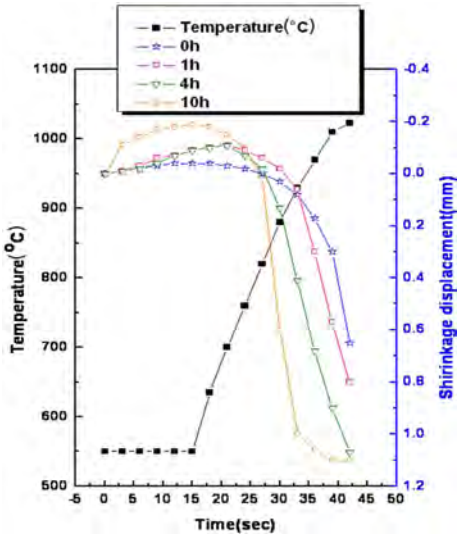

Fig. 4. Shrinkage displacement-temperature curve during the pulsed current activated sintering of TiO_2 powders milled for various durations.

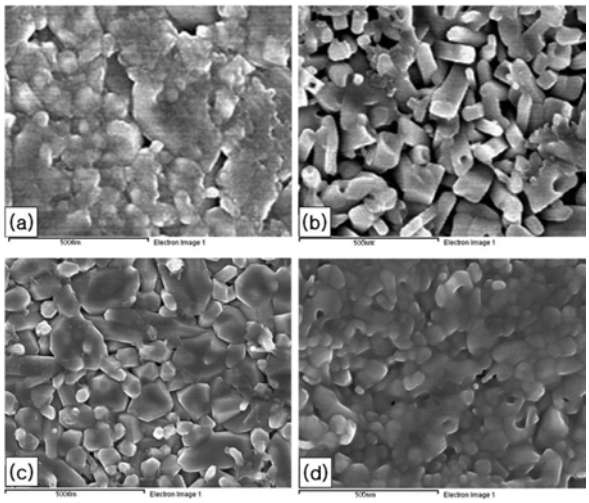

Fig. 6. FE-SEM micrographs showing the polished and etched surface of TiO_2 compacts: (a) as-received (b) milled for 1 h, (c) milled for 4 h, and (d) milled for 10 h.

depends on the milling conditions. The amount of shrinkage displacement, which should be indication of densification degree, increases with the milling time. It is clearly seen that the shrinkage-start temperature decreases as the milling time increases. The as-received TiO_2 powders started to shrink after about 25 s which corresponds to 800 °C. In contrast, TiO_2 powders milled for 10 h start to shrink at a much lower temperature of 650 °C. This demonstrates the effectiveness of prior-milling on the densification of TiO_2 powders. A high-energy ball milling treatment allows the control of the formation of the compound by fixing the reactant powder microstructure. Indeed, high-energy ball milling produces finer crystallites, more strain and defects. Therefore, the consolidation temperature decreases with milling time because the driving force for sintering and contact points of powders for atomic diffusion increases.

Microstructure of TiO_2 compact

Fig. 5 shows the X-ray diffraction patterns of TiO_2 sintered from various milled powders. All peaks are TiO_2 and their peak broadening was seen to reduce suggesting that there would be some grain growth during sintering. Fig. 6(a-d) shows SEM images of polished surface of the sintered TiO_2 compact. The reduction of pore volume with milling time is obvious. It became dense and had more refined microstructure as the milling time increases. The microstructural refinement can be better recognized on the fracture surface. Fig. 7(a-d)

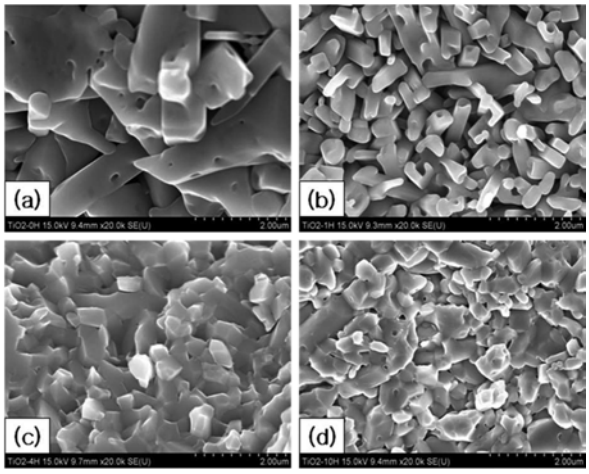

Fig. 7. SEM micrographs showing the fracture surface of TiO_2 compacts: (a) as-received (b) milled for 1 h, (c) milled for 4 h, and (d) milled for 10 h.

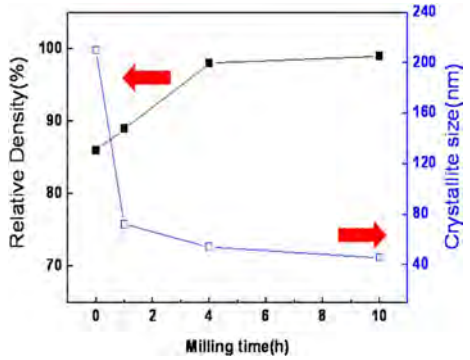

Fig. 8. Variation of relative density and grain size of TiO_2 sintered from various milled powders.

shows the SEM micrographs showing the intergranular-type fracture surface of sintered TiO_2 compact. It is obvious that the crystallite size becomes finer as the milling time increases.

Fig. 8 shows the effect of milling on the crystallite size and relative density for sintered compacts. The crystallite size is seen to decrease significantly by milling and the relative density increases by milling. The crystallite size became larger during sintering suggesting that some grain growth occurred. Nevertheless, the average crystallite size of the sintered TiO_2 is not greatly larger than that of the milled powders and is still in the nano-scale realm. The retention of the nanoscale crystallite size might be attributed to the high heating rate and the relatively short exposure time of the powders to high temperature in PCAS. The role of the current (resistive or inductive) in sintering has been the focus of several attempts aimed at providing an explanation of the observed enhancement of sintering and the improved characteristics of the products. The role played by the current has been variously interpreted, the effect being explained in terms of a fast heating rate due to Joule heating, the presence of a plasma in pores separating powder particles, and the

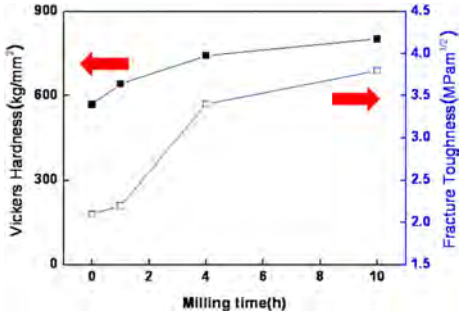

Fig. 9. Variation of hardness and fracture toughness of TiO2 sintered from various milled powders.

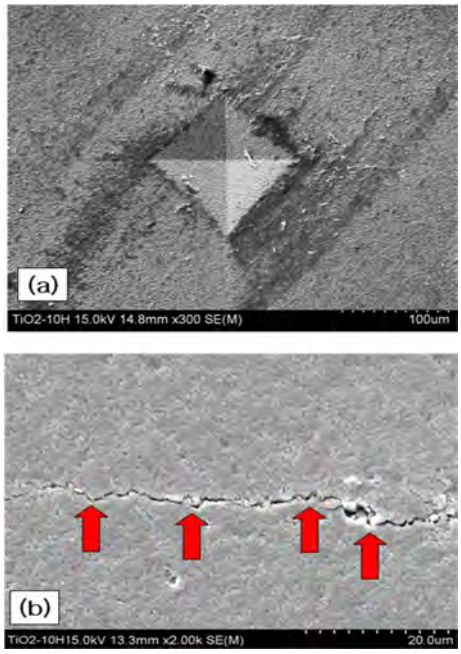

Fig. 10. (a) Vickers hardness indentation and (b) median crack propagating of TiO_2 sintered from milled powder for 10 h.

intrinsic contribution of the current to mass transport [24-27].

Mechanical properties of TiO_2 compact

Vickers hardness and fracture toughness was measured to evaluate the mechanical properties of TiO_2 compact. Vickers hardness measurements were performed on polished sections of the TiO_2 samples using a 10 kg_f load and 15 s dwell time. Indentations with large enough loads produced radial cracks emanating from the corners of the indent. The lengths of these cracks permit estimation of the fracture toughness of the materials by means of the expression [28]:

$$K_{IC} = 0.203(c/a)^{-3/2} \cdot H_v \cdot a^{1/2} \quad (2)$$

where c is the trace length of the crack measured from the center of the indentation, a is one half of the average length of the two indent diagonals, and H_v is the hardness.

Fig. 9 shows the hardness and fracture toughness of TiO_2 sintered from various milled powders. The hardness and fracture toughness increased as the milling time increased. This effect may be attributed to the refined microstructure and/or higher density. Vickers hardness indentation and a higher magnification view of the indentation median crack in a TiO_2 sample sintered from milled powder for 10h is shown in Fig. 10, which shows that the crack propagated deflectively (↑).

Summary

TiO_2 powders were high-energy ball milled for various durations and consolidated using the pulsed current activated sintering (PCAS). The ball milling substantially refined the crystallite structure of TiO_2 powders and facilitated the subsequent densification process. The consolidation temperature of TiO_2 powders was reduced by milling because the driving force for sintering and contact points of powders for atomic diffusion increases.

The milling for 10 h reduced the crystallite size from 206 nm to 20 nm. The rapid consolidation of the PCAS process retained the nanostructure after sintering. The microhardness and fracture toughness of TiO_2 sintered from powders milled for 0, 1, 4, and 10 h were 568, 642, 743 , 802 kg/mm^2 and 2.2, 2.2, 3.4, 3.8 MPa · m$^{1/2}$.

Acknowledgment

This work is partially supported by KIST Future Resource Research Program and this research was supported by the Basic Science Research Program through the National Research Foundation of Korea (NRF), funded by the Ministry of Education, Science and Technology (No. 2012001300).

References

1. K. Iketani, R.D. Sun, M. Toki, K. Hirota and O. Yamaguchi, J. Phys. Chem. Solids 64 (2003) 507-513.
2. C.J. Barbé, F. Arendse, P. Comte, M. Jirousek, F. Lenzmann, V. Shklover and M. Grätzel, J. Am. Ceram. Soc. 80 [3157] (1997) 3157-3171.
3. C. Garzella, E. Comini, E. Bontempi, L.E. Depero, C. Frigeri and G. Sberveglieri, Sens. Actuators B 83 (2002) 230-237.
4. D.J. Kim, S.H. Hahn, S.H. Oh and E.J. Kim, Mater. Lett. 57 (2002) 355-360.
5. D. Qin, W. Chang, J. Zhou and Y. Chen, Thermochim. Acta 236 (1994) 205-216.
6. H. Gleiter, Nanostructured Materials 6 (1995) 3-7.
7. J.R. Yoon, D.J. Choi, K.H. Lee, J.Y. Lee, Y.H. Kim, Electron. Mater. Lett. 4 (2008) 167-172.
8. J. Karch, R. Birringer, and H. Gleiter, Nature 330 (1987) 556-558.
9. A.M. George, J. Iniguez, and L. Bellaiche, Nature 413 (2001) 54-57.
10. D. Hreniak, and W. Strek, Journal of Alloys and Compounds 341 (2002) 183-186.
11. C. Xu, J. Tamaki, N. Miura, and N. Yamazoe, Sensors and Actuators B: Chemical 3 (1991) 147-155.
12. D.G. Lamas, A. Caneiro, D. Niebieskikwiat, R.D. Sanchez. D. Garcia, and B. Alascio, Journal of Magnetism and Magnetic Materials 241 (2002) 207-213.
13. C.W. Nahm, C.J. Kim, Y.J. Park, B.J. Lee, and B.W. Park, Electron. Mater. Lett. 4 [5] (2008) 5-8.
14. E.S. Ahn, N.J. Gleason, A. Nakahira, and J.Y. Ying, Nano Letters 1 (2001) 149-153.
15. Z. Fang, J.W. Eason, Int. J. of Refractory Met. & Hard Mater 13 (1995) 297-302.
16. S.L. Du, S.H. Cho, I.Y. Ko, J.M. Doh, J.K. Yoon, S.W. Park, I.J. Shon, Kor. J. Met. Mater 49 (2011) 231-236.
17. N.R. Park, I.Y. Ko, J.M. Doh, J.K. Yoon, I.J. Shon, Journal of Ceramic Processing Research 12 (2011) 660-663.
18. S.C. Liao, W.E. Mayo, K.D. Pae, Acta Mater 45 (1997) 4027-4032.
19. Z.Q. Jin, C. Rockett, J.P. Liu, K. Hokamoto, N.N. Thadhani, Mater Sci Forum 465-466 (2004) 93-97.
20. V. Ivanov, S. Paranin, V. Khrustov, A. Medvedev, A. Shtolts, Key Eng Mater 206-213 (2002) 377-381.
21. H.S. Kang, I.Y. Ko, J.K. Yoon, J.M. Doh, K.T. Hong, I.J. Shon, Metals and Materials International 17 (2011) 57-62.
22. I.Y. Ko, I.J. Shon, J.M. Doh, J.k. Yoon, S.W. Park, N.R. Park, Journal of Ceramic Processing Research 12 (2011) 70-73.
23. C. Suryanarayana, M. Grant Norton, X-ray Diffraction A Practical Approach, Plenum Press, New York (1998).
24. Z. Shen, M. Johnsson, Z. Zhao and M. Nygren, J. Am. Ceram. Soc. 85 [1921] (2002) 1921-27.
25. J.E. Garay, U. Anselmi-Tamburini, Z.A. Munir, S.C. Glade and P. Asoka- Kumar, Appl. Phys. Lett. 85 (2004) 573-75.
26. J.R. Friedman, J.E. Garay, U. Anselmi-Tamburini and Z.A. Munir, Intermetallics 12 (2004) 589-97.
27. J.E. Garay, U. Anselmi-Tamburini and Z.A. Munir, Acta. Mater. 51 (2003) 4487-95.
28. K. Niihara, R. Morena, and D.P.H. Hasselman, J. Mater. Sci. Lett. 1 (1982) 12-16.